Journal of Ultrafine Grained and Nanostructured Materials
https://jufgnsm.ut.ac.ir
Vol. 50, No.1, June 2017, pp. 60-80
Print ISSN: 2423-6845 Online ISSN: 2423-6837
DOI: 10.7508/jufgnsm.2017.01.08

Multiscale Evaluation of the Nonlinear Elastic Properties of Carbon Nanotubes Under Finite Deformation

Abolfazl Shahabodini[1], Reza Ansari*[,1], Mansour Darvizeh[1]

[1]Department of Mechanical Engineering, University of Guilan, P.O. Box 3756, Rasht, Iran.

Recieved: 28 February 2017; Accepted: 5 May 2017
** Corresponding author email: r_ansari@guilan.ac.ir*

ABSTRACT

This paper deals with the calculation of the elastic properties for single-walled carbon nanotubes (SWCNTs) under axial deformation and hydrostatic pressure using the atomistic-based continuum approach and the deformation mapping technique. A hyperelastic model based on the higher-order Cauchy-Born (HCB) rule being applicable at finite strains and accounting for the chirality and material nonlinearity is presented. Mechanical properties of several carbon nanotubes (CNTs) are computed and compared with the existing theoretical results and a good agreement is observed. Moreover, by comparison with atomistic calculations, it is found that the present model can reproduce the energetics of axially deformed CNTs. The model is then adopted to study the dependence of the elastic properties on chirality, radius and strain which yields an upper bound on the stability limit of axially and circumferentially stretched nanotubes. The influence of chirality is found to be more prominent for smaller tubes and as the diameter increases, the anisotropy induced by finite deformations gets nullified. It is discerned that the constitutive properties of the CNT can vary with deformation in a nonlinear manner. It is also found that the CNT displays a martial softening behavior at finite tensile strains and a hardening behavior at slightly compressive strains.

Keywords: *Elastic properties; Carbon nanotube; Multiscale modeling; Higher-order Cauchy-Born rule; Finite deformation.*

How to cite this article:
Shahabodini A, Ansari R, Darvizadeh M. Multiscale Evaluation of the Nonlinear Elastic Properties of Carbon Nanotubes Under Finite Deformation. J Ultrafine Grained Nanostruct Mater, 2017; 50(1):60-80.
DOI: 10.7508/jufgnsm.2017.01.08

1. Introduction

Thanks to their outstanding mechanical and electronic properties [1-3], carbon nanotubes hold great promise for numerous applications in nano-structured materials, nano-electromechanical systems, molecular electronics, nanocomposites and etc. Carbon nanotubes are known to be capable of sustaining large elastic deformations without developing lattice defects [4].

To make proper use of these nanomaterials, a good knowledge of their mechanical properties is desperately required. A number of experimental and theoretical studies have been conducted to explore the mechanical properties of carbon nanotubes and graphene sheets (GSs). Some primary experimental works concerning the measurement of the elastic properties of CNTs can be found in [5-10]. However, as well known, due to very small size of the structure at nanoscale, direct determination of the mechanical properties in experiment is very difficult.

Different atomistic modeling approaches such as

tight-binding models [11-13], ab initio calculations [14-16], simulations based on analytical potentials [17-30] have been developed to extract elastic constitutive properties. Molecular dynamics (MD) simulations with the Tersoff-Brenner interatomic potential for carbon [17, 19-21] and other potential functions such as Keating potential [18], summation of pairwise harmonic potentials [22] and the potential considering both the stretch in bond length and change in bond angle [23, 24] have been adopted by the researchers and a large variation of Young's modulus has been reported. Recently, Li et al. [30] made a comparison between the mechanical and thermal properties of single-walled carbon nanotubes and boron nitride nanotubes performing MD simulations with the parameterized Tersoff potentials. In these physics-based methods, approximate polynomial fits or numerical approximation of derivatives in the extraction of the elastic moduli lead to significant numerical errors [4]. Moreover, the atomic modeling techniques are time-consuming and restricted to small-sized structures having a small number of molecules or atoms.

As the dimensions of a structure diminish to a very small scale (e.g., micro/nanoscale), the size effects become significant. Modified (non-classical) continuum theories such as the nonlocal elasticity theory [31, 32], couple stress theory [33, 34] and strain gradient theory [35, 36] account for the size effects by incorporating length scale parameters into the constitutive relations. In this respect, Wang et al. [37] developed a size-dependent beam model based on the nonlocal elasticity and Timoshenko beam theories to consider the small scale and transverse shear deformation effects in the free vibration analysis of micro\nanobeams. The effect of nonlocality on the static deflection, critical buckling load and natural frequencies of CNTs was described by Reddy and Pang [38] through incorporating Eringen's elasticity theory into the Euler–Bernoulli and Timoshenko beam theories. Hu et al. [39] analyzed the transverse and torsional wave propagations in single- and double-walled CNTs by a nonlocal elastic cylindrical shell model. They also used MD simulations to calibrate the scale coefficient for the nonlocal model. On the basis of the thermal elasticity mechanics and Eringen's nonlocal constitutive relations, Murmu and Pradhan [40] studied the thermal vibration of single-walled carbon nanotubes embedded in an elastic matrix. Civalek et al. [41] employed the differential quadrature approach to simulate the nonlocal bending of carbon nanotubes with different boundary conditions. Based on von Kármán geometric nonlinearity, Timoshenko and nonlocal elasticity theories, Yang et al [42] modeled single-walled carbon nanotubes as nanobeams and analyzed the nonlinear free vibration of them. Lim and Yang [43] presented an exact nonlocal model for wave propagation in carbon nanotubes according to the variational principal and the Euler-Bernoulli model. Akgöz and Civalek [44] presented analytical solutions accounting for the scale influence for the buckling of clamped-free carbon nanotubes employing the modified strain gradient and couple stress theories. An analytical Euler–Bernoulli beam model considering the nonlocality was proposed by Yang et al. [45] to describe the wave propagation in fluid-filled SWCNTs. Demir and Civalek [46] derived finite element formulation for vibrations of Euler-Bernoulli nanobeams axially compressed and embedded in elastic medium using the nonlocal elasticity. They [47] also developed a nonlocal beam model taking the size effect into account for elastic stability of microtubules surrounded by an elastic matrix. The finite element method was adopted for doing numerical calculations. Akgöz and Civalek [48] analytically investigated the bending response of simply-supported carbon nanotubes resting on an elastic foundation in the framework of the modified strain gradient elasticity and higher-order shear deformation beam theories.

The aforementioned full continuum models suffer from some shortcomings as follows [49]. They introduce Young's modulus and thickness concept for the carbon nanotube in building the stiffness matrix whose values are scattered in the literature. Moreover, these models depend on extra material constants which need fitting of experimental or atomistic simulations results to properly be determined. Further, the continuum beam or shell models ignore the material nonlinearity due to the bond interactions [49].

Another class of the theoretical approaches overcoming the limitations of full atomistic and full continuum models is the coupled atomistic-continuum method based on the Cauchy-Born rule. In these methods, the atomistic information are directly incorporated into the constitutive law at the continuum level i.e., the constitutive properties are obtained from the underlying lattice. Carbon nanotube is modeled as a curved two-dimensional crystalline membrane without thickness. Hence,

the ambiguous issue of the definition of thickness and the parameter fitting process involved in the non-classical continuum theories are bypassed. The model on the basis of the Cauchy-Born rule is capable of describing the mechanics of crystals at finite strains [50]. Zhang et al. [51] developed a nanoscale continuum theory based on the standard Cauchy-Born rule to estimate linear elastic modulus of carbon nanotube without accounting for the effect of initial curvature. A finite deformation continuum theory using the exponential Cauchy-Born rule was developed by Arroyo and Belytschko [50, 52, 53] to study the elastic properties and large deformation of carbon nanotubes. Effect of radius on Young's modulus of armchair and zigzag CNTs was studied by Jiang et al. [54] using a continuum analysis incorporating the interatomic potential. Jiang et al. [55] developed a finite-temperature continuum theory based on the interatomic potentials to describe the temperature dependence of the material properties of graphene and diamond. Guo et al. [56] and Wang et al. [57] incorporated the second-order deformation gradient into the kinematic description and proposed a higher-order Cauchy-Born rule. The energy, mechanical properties such as Young's modulus, Poisson's ratio [56, 57] and bending stiffness [57] of carbon nanotubes were investigated. With the use of an atomistically enriched continuum analysis, Chandraseker and Mukherjee [4] calculated shear and Young's moduli of CNTs under coupled extension and twist deformations. Considering SWCNTs as crystal membranes without thickness, a closed-form formula for the bending stiffness of SWCNTs was derived by Guo and Zhang [58] using the molecular mechanics model and the deformation mapping technique. Guo et al. [59] established a nanoscale quasi-continuum constitutive model based on the temperature-related higher-order Cauchy–Born rule to investigate the thermo-mechanical properties of single-walled carbon nanotubes. Ansari et al. [60-64] calculated the constitutive properties for the nonlocal continuum modeling of GSs [60-62] and carbon nanotubes [63, 64] from the underlying lattice. They used the standard Cauchy-Born rule to establish a linkage between the strain energy induced in the continuum and the interatomic potential. Some researchers employed nanoscale continuum models wherein the carbon-carbon bond is replaced by a continuum element (such as truss, spring and beam) and evaluated the mechanical properties of CNTs [65-68].

Owing to the nonlinear interatomic interactions, the CNTs and GSs display a nonlinear material behavior [69]. This necessitates the knowledge of the elastic properties of these nanostructures at finite strains. However, few works have been carried out on the elastic behavior of the carbon nanotubes and graphene sheets under finite deformation. Zhou and Huang [70] used a MD approach to study the internal relaxation and elastic moduli of single layer graphene sheet subject to in-plane deformation. Extensional stiffness coefficients of graphene were investigated by Lu and Huang [71] using molecular dynamics simulation with second generation reactive empirical bond order (REBO) potential. Strong anisotropy was found for the in-plane moduli of a graphene sheet under finite stretches. Lu et al. [72] proposed analytical formulae for the elastic bending modulus of GS based on an empirical potential. They investigated the influence of curvature on bending modulus of GS subject to cylindrical bending at finite curvatures. Employing an atomistic–continuum multiscale approach, in which the deformed bond length was considered as a function of in-plane strains and curvatures, Singh and Patel [69] evaluated the effect of different combinations of induced strain/curvature on stiffness coefficients of graphene sheets.

To the best of the authors' knowledge, the elastic properties of a carbon nanotube under finite deformation have not been evaluated using multiscale analysis based on the higher-order Cauchy-Born rule. In this paper, the elastic material properties of CNTs under tension, compression and hydrostatic pressure are studied by the use of a membrane theory. The overall deformation of SWCNTs is described via smooth mapping functions defined on the planar GS. The strain energy of the membrane is written in closed-form exclusively in terms of the interatomic potentials in the framework of the HCB rule. This enables one to derive analytical expressions for the elastic moduli in terms of the atomistic potential. The resulting constitutive model does not involve any additional phenomenological input and is a finite deformation model in nature. Selected results are first compared with those of other multiscale approaches and atomistic calculations available in the literature to verify the validity of the present analysis. Afterward, the model is employed to describe the energetics and elastic properties of carbon nanotubes at the equilibrium state and at

finite axial and circumferential strains.

2. Hyperelastic constitutive model

In this paper, the higher-order Cauchy–Born rule is adopted to link the deformation of the atomistic crystalline lattice to that of the continuum field. Using this rule, a hyperelastic strain energy density induced in the continuum is formulated from the bond energies over a representative cell of the atomic lattice. The undeformed or reference system $\forall_0$ is considered to be the planar graphene sheet replaced herein by a rectangular continuum surface without thickness (or actually, a surface of one atom thickness). The atoms are assumed to lie on the surface and the bonds are chords of it.

2.1. Continuum strain energy density

The higher-order Cauchy–Born rule accounts for the bending and original curvature of the crystal effects by incorporating the second-order deformation gradient into the kinematic description of deformation of the CNT. This causes the strain energy density to be dependent on both the first- and second-order deformation gradients and so, the resulting constitutive model to be much closer to the reality. Let $\mathbf{A}_{IJ}$ denote the lattice vector between atoms I and J in the reference configuration and $\mathbf{a}_{IJ}$ be the deformed vector in the current configuration. According to the HCB rule, the deformation of the lattice vector in the crystal is connected to the continuum deformation field as

$$\mathbf{a}_{IJ} = \mathbf{F}\cdot(\mathbf{A}_{IJ}+\boldsymbol{\eta}) + \frac{1}{2}\mathbf{G}:\left((\mathbf{A}_{IJ}+\boldsymbol{\eta})\otimes(\mathbf{A}_{IJ}+\boldsymbol{\eta})\right) \quad \text{(Eq. 1)}$$

Where $\mathbf{F}$ and $\mathbf{G}$ stand for the first-order and second-order deformation gradients, respectively. The vector $\boldsymbol{\eta}=(\boldsymbol{\eta}_1,\boldsymbol{\eta}_2)$ is an inner relaxation parameter considered between two simple Bravais lattices in the reference configuration [50-53], as shown in Fig. 1, to ensure the internal equilibrium of the deformed graphene sheet and CNT.

To reflect the interatomic interactions, the Tersoff-Brenner multi-body potential [73, 74] is employed according to which the bond energy between atoms and is evaluated as

$$V(a_{IJ}) = V_R(a_{IJ}) - B_{IJ}V_A(a_{IJ}) \quad \text{(Eq. 2)}$$

where a_{IJ} denotes the bond length. B_{IJ} indicates a multi-body coupling between the interatomic bond I-J and the local environment of atom I, V_R and V_A are the pair-additive repulsive and attractive interaction terms, respectively given by

$$V_R(a_{IJ}) = \frac{D^{(e)}}{S-1}e^{-\sqrt{2S}\beta(a_{IJ}-R^{(e)})}f_c(a_{IJ}) \quad \text{(Eq. 3)}$$

$$V_A(a_{IJ}) = \frac{D^{(e)}S}{S-1}e^{-\sqrt{2/S}\beta(a_{IJ}-R^{(e)})}f_c(a_{IJ}) \quad \text{(Eq. 4)}$$

$$B_{IJ} = \left(1+\sum\nolimits_{K(\neq I,J)} G(\theta_{IJK})f_c(a_{IK})\right)^{-\delta} \quad \text{(Eq. 5)}$$

in which denotes atoms except I and J. a_{IK} is the bond length between atoms I and K and θ_{IJK} represents the angle between bonds I-J and I-K. The cut-off function f_c and the angle function $G(\theta_{IJK})$ are of the following form

$$f_c(a) = \begin{cases} 1, & a < R^{(1)} \\ \frac{1}{2}\left\{1+\cos\left[\frac{\pi(a-R^{(1)})}{R^{(2)}-R^{(1)}}\right]\right\} & R^{(1)} < a < R^{(2)} \\ 0, & a > R^{(2)} \end{cases} \quad \text{(Eq. 6)}$$

$$G(\theta_{IJK}) = a_0\left(1+\frac{{c_0}^2}{{d_0}^2}-\frac{{c_0}^2}{{d_0}^2+(1+\cos\theta_{IJK})^2}\right) \quad \text{(Eq. 7)}$$

Two sets of the parameters for the Brenner potential are reported and the second set is employed in the present work [74]. Deformation energy of a representative cell is obtained by the total of the bond energies within the cell. The average volume strain energy density can be determined by equating the strain energy of the cell to energy of an equivalent volume of the continuum. Considering the representative cell depicted in Fig.1 and assuming that the energy of the atom I, V_I, can be homogenized over the cell, the strain energy density of the continuum membrane is obtained by [56]

$$W(\mathbf{F},\mathbf{G},\boldsymbol{\eta}) = W(a_{I1},a_{I2},a_{I3}) = \frac{V_I}{\forall_c} =$$

$$\frac{1}{2\forall_c}\sum_{J=1}^{3}V_{IJ}(a_{I1},a_{I2},a_{I3}) = \sum_{J=1}^{3}V_{IJ}(\mathbf{F},\mathbf{G},\boldsymbol{\eta}) \quad \text{(Eq. 8)}$$

Where $\forall_c$ represents the average area

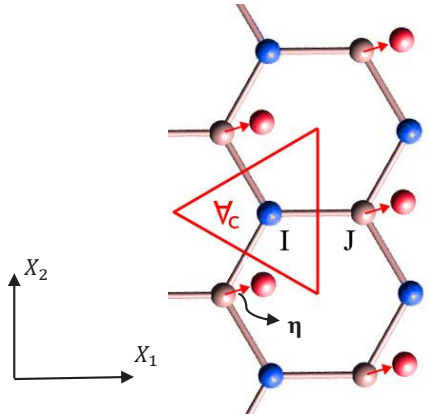

Figure 1: Two simple Bravais lattices represented in different colors are relatively displaced by the shift vector $\boldsymbol{\eta}$. The representative cell of area $\forall_c$ is also indicated.

per atom in the reference configuration as $\forall_c = 3\sqrt{3}/4(a_0)^2$ in which a_0=0.145 nm is the equilibrium bond length in graphene. The inner relaxation parameter is a function of **F** and **G** determined by minimizing the energy of atom. So, for a given finite deformation characterized by **F** and **G**, the inner displacements are additional kinematic variables that can be eliminated at the constitutive level by minimization of the strain energy density with respect to η as

$$\hat{\boldsymbol{\eta}} = arg\left(\min_{\boldsymbol{\eta}} W(\mathbf{F},\mathbf{G},\boldsymbol{\eta})\right) \rightarrow$$

$$\left.\frac{\partial W}{\partial \boldsymbol{\eta}}\right|_{\boldsymbol{\eta}=\hat{\boldsymbol{\eta}}} = \left.\frac{\partial V_I}{\partial \boldsymbol{\eta}}\right|_{\boldsymbol{\eta}=\hat{\boldsymbol{\eta}}} = \mathbf{0} \qquad \text{(Eq. 9)}$$

In general, **η** cannot be calculated analytically and the minimization problem in Eq. (9) is numerically solved. After the equilibrium value of **η** is obtained, the effective strain energy density (i.e., the energy at the relaxed inner displacement) can be expressed in terms of **F** and **G** only

$$\widehat{W}(\mathbf{F},\mathbf{G}) = W\big(\mathbf{F},\mathbf{G},\hat{\boldsymbol{\eta}}(\mathbf{F},\mathbf{G})\big) \qquad \text{(Eq. 10)}$$

2.2. Constitutive relation

The first Piola-Kirchhoff stress tensor $\widehat{\mathbf{P}}$ and the higher-order stress tensor $\widehat{\mathbf{Q}}$ are obtained by differentiating the strain energy density function with respect to the first- and second-order deformation gradient tensors, respectively as

$$\widehat{\mathbf{P}} = \frac{\partial \widehat{W}}{\partial \mathbf{F}} = \left.\frac{\partial W}{\partial \mathbf{F}}\right|_{\boldsymbol{\eta}=\hat{\boldsymbol{\eta}}} =$$

$$\frac{1}{2\forall_c}\sum_{J=1}^{3}\left(\left(V_R' - B_{IJ}V_A'\right)\frac{\partial a_{IJ}}{\partial \mathbf{F}} - \frac{\partial B_{IJ}}{\partial \mathbf{F}}V_A\right)\Big|_{\boldsymbol{\eta}=\hat{\boldsymbol{\eta}}} \qquad \text{(Eq. 11-a)}$$

$$\widehat{\mathbf{Q}} = \frac{\partial \widehat{W}}{\partial \mathbf{G}} = \left.\frac{\partial W}{\partial \mathbf{G}}\right|_{\boldsymbol{\eta}=\hat{\boldsymbol{\eta}}} =$$

$$\frac{1}{2\forall_c}\sum_{J=1}^{3}\left(\left(V_R' - B_{IJ}V_A'\right)\frac{\partial a_{IJ}}{\partial \mathbf{G}} - \frac{\partial B_{IJ}}{\partial \mathbf{G}}V_A\right)\Big|_{\boldsymbol{\eta}=\hat{\boldsymbol{\eta}}} \qquad \text{(Eq. 11-b)}$$

where ´ symbols the first-order derivative with respect to a_{IJ}. For given deformation gradients **F** and **G**, the above equations result in the stresses **P** and **Q** at the relaxed inner displacements. In other words, Eqs. (11a-b) give the constitutive law of carbon nanotubes in terms of the deformation gradients and the first Piola-Kirchhoff and higher-order stresses under mechanical deformation. Subsequently, with regard to Eq. (9), the effective tangent modulus tensors can be obtained by taking second-order derivatives of the strain energy density with respect to the deformation gradients as

$$\widehat{\mathbf{M}}^{FF} = \frac{\partial^2 \widehat{W}}{\partial \mathbf{F}\partial \mathbf{F}} = \left.\frac{\partial^2 W}{\partial \mathbf{F}\partial \mathbf{F}}\right|_{\boldsymbol{\eta}=\hat{\boldsymbol{\eta}}} -$$

$$\left(\frac{\partial^2 W}{\partial \mathbf{F}\partial \boldsymbol{\eta}}\cdot\left(\frac{\partial^2 W}{\partial \boldsymbol{\eta}\partial \boldsymbol{\eta}}\right)^{-1}\cdot\frac{\partial^2 W}{\partial \boldsymbol{\eta}\partial \mathbf{F}}\right)\Big|_{\boldsymbol{\eta}=\hat{\boldsymbol{\eta}}}, \qquad \text{(Eq. 12-a)}$$

$$\widehat{\mathbf{M}}^{FG} = \frac{\partial^2 \widehat{W}}{\partial \mathbf{F}\partial \mathbf{G}} = \left.\frac{\partial^2 W}{\partial \mathbf{F}\partial \mathbf{G}}\right|_{\boldsymbol{\eta}=\hat{\boldsymbol{\eta}}} -$$

$$\left(\frac{\partial^2 W}{\partial \mathbf{F}\partial \boldsymbol{\eta}}\cdot\left(\frac{\partial^2 W}{\partial \boldsymbol{\eta}\partial \boldsymbol{\eta}}\right)^{-1}\cdot\frac{\partial^2 W}{\partial \boldsymbol{\eta}\partial \mathbf{G}}\right)\Big|_{\boldsymbol{\eta}=\hat{\boldsymbol{\eta}}}, \qquad \text{(Eq. 12-b)}$$

$$\widehat{\mathbf{M}}^{GF} = \frac{\partial^2 \widehat{W}}{\partial \mathbf{G}\partial \mathbf{F}} = \left.\frac{\partial^2 W}{\partial \mathbf{G}\partial \mathbf{F}}\right|_{\boldsymbol{\eta}=\hat{\boldsymbol{\eta}}} -$$

$$\left(\frac{\partial^2 W}{\partial \mathbf{G}\partial \boldsymbol{\eta}}\cdot\left(\frac{\partial^2 W}{\partial \boldsymbol{\eta}\partial \boldsymbol{\eta}}\right)^{-1}\cdot\frac{\partial^2 W}{\partial \boldsymbol{\eta}\partial \mathbf{F}}\right)\Big|_{\boldsymbol{\eta}=\hat{\boldsymbol{\eta}}}, \qquad \text{(Eq. 12-c)}$$

$$\widehat{\mathbf{M}}^{GG} = \frac{\partial^2 \widehat{W}}{\partial \mathbf{G}\partial \mathbf{G}} = \left.\frac{\partial^2 W}{\partial \mathbf{G}\partial \mathbf{G}}\right|_{\boldsymbol{\eta}=\hat{\boldsymbol{\eta}}} -$$

$$\left(\frac{\partial^2 W}{\partial \mathbf{G}\partial \boldsymbol{\eta}}\cdot\left(\frac{\partial^2 W}{\partial \boldsymbol{\eta}\partial \boldsymbol{\eta}}\right)^{-1}\cdot\frac{\partial^2 W}{\partial \boldsymbol{\eta}\partial \mathbf{G}}\right)\Big|_{\boldsymbol{\eta}=\hat{\boldsymbol{\eta}}}. \qquad \text{(Eq. 12-d)}$$

The derivatives of the strain energy density in the previous equations can be expressed in terms of the first- and second-order derivatives of the elastic interatomic potential and the deformed bond length. For example, the derivative terms in Eq. (12a) are expanded in the following form

$$\frac{\partial^2 W}{\partial \mathbf{F}\partial \mathbf{F}} = \frac{1}{2\forall_c}\sum_{J=1}^{3}\left(\left(V_R'' - B_{IJ}V_A''\right)\frac{\partial a_{IJ}}{\partial \mathbf{F}}\otimes\frac{\partial a_{IJ}}{\partial \mathbf{F}} +,\right.$$

$$\left(V_R' - B_{IJ}V_A'\right)\frac{\partial^2 a_{IJ}}{\partial \mathbf{F}\partial \mathbf{F}} -$$

$$\left.V_A'\left(\frac{\partial B_{IJ}}{\partial \mathbf{F}}\otimes\frac{\partial a_{IJ}}{\partial \mathbf{F}} + \frac{\partial r_{IJ}}{\partial \mathbf{F}}\otimes\frac{\partial B_{IJ}}{\partial \mathbf{F}}\right) - V_A\frac{\partial^2 B_{IJ}}{\partial \mathbf{F}\partial \mathbf{F}}\right) \qquad \text{(Eq. 13-a)}$$

$$\frac{\partial^2 W}{\partial \mathbf{F}\partial \boldsymbol{\eta}} = \frac{1}{2\forall_c}\sum_{J=1}^{3}\left(\left(V_R'' - B_{IJ}V_A''\right)\frac{\partial a_{IJ}}{\partial \mathbf{F}}\otimes\frac{\partial a_{IJ}}{\partial \boldsymbol{\eta}} +\right.$$

$$\left(V_R' - B_{IJ}V_A'\right)\frac{\partial^2 a_{IJ}}{\partial \mathbf{F}\partial \boldsymbol{\eta}} -$$

$$\left.V_A'\left(\frac{\partial B_{IJ}}{\partial \mathbf{F}}\otimes\frac{\partial a_{IJ}}{\partial \boldsymbol{\eta}} + \frac{\partial a_{IJ}}{\partial \mathbf{F}}\otimes\frac{\partial B_{IJ}}{\partial \boldsymbol{\eta}}\right) - V_A\frac{\partial^2 B_{IJ}}{\partial \mathbf{F}\partial \boldsymbol{\eta}}\right) \qquad \text{(Eq. 13-b)}$$

$$\frac{\partial^2 W}{\partial \boldsymbol{\eta}\partial \mathbf{F}} = \frac{1}{2\forall_c}\sum_{J=1}^{3}\left(\left(V_R'' - B_{IJ}V_A''\right)\frac{\partial a_{IJ}}{\partial \boldsymbol{\eta}}\otimes\frac{\partial a_{IJ}}{\partial \mathbf{F}} +\right.$$

$$\left(V_R' - B_{IJ}V_A'\right)\frac{\partial^2 a_{IJ}}{\partial \boldsymbol{\eta}\partial \mathbf{F}} -$$

$$\left.V_A'\left(\frac{\partial a_{IJ}}{\partial \boldsymbol{\eta}}\otimes\frac{\partial B_{IJ}}{\partial \mathbf{F}} + \frac{\partial B_{IJ}}{\partial \boldsymbol{\eta}}\otimes\frac{\partial a_{IJ}}{\partial \mathbf{F}}\right) - V_A\frac{\partial^2 B_{IJ}}{\partial \boldsymbol{\eta}\partial \mathbf{F}}\right) \qquad \text{(Eq. 13-c)}$$

in which the symbol '' indicates the second-order derivative with respect to a_{IJ}. Using Eqs. (12a-d), one can write the incremental form of the constitutive relation for CNTs as

$$\dot{\hat{\mathbf{P}}} = \hat{\mathbf{M}}^{FF} : \dot{\mathbf{F}} + \hat{\mathbf{M}}^{FG} \vdots \dot{\mathbf{G}} \quad \text{(Eq. 14-a)}$$

$$\dot{\hat{\mathbf{Q}}} = \hat{\mathbf{M}}^{GF} : \dot{\mathbf{F}} + \hat{\mathbf{M}}^{GG} \vdots \dot{\mathbf{G}} \quad \text{(Eq. 14-b)}$$

It should be noted that in contrast with the planar graphene, the tangent modulus tensors for CNTs appeared in the previous relationships are no longer isotropic. So, Eqs. (14a-b) are nonlinear and take the anisotropy of carbon nanotubes into account. For the infinitesimal deformations, the strain energy density can be stated in a quadratic form in terms of the deformation gradients as

$$\hat{W} = \hat{W}_0 + \frac{1}{2}(\mathbf{F} : \hat{\mathbf{M}}_0^{FF} : \mathbf{F} + \mathbf{G} \vdots \hat{\mathbf{M}}_0^{GG} \vdots \mathbf{G} + \mathbf{F} : \hat{\mathbf{M}}_0^{FG} \vdots \mathbf{G} + \mathbf{G} \vdots \hat{\mathbf{M}}_0^{GF} : \mathbf{F}) \quad \text{(Eq. 15)}$$

where $\hat{W}_0$ is the initial strain energy density of the carbon nanotube prior to deformation. Also, $\hat{\mathbf{M}}_0^{FF}$, $\hat{\mathbf{M}}_0^{GG}$, $\hat{\mathbf{M}}_0^{FG}$ and $\hat{\mathbf{M}}_0^{GF}$ are the linear or infinitesimal effective elastic moduli that can be obtained by taking a vanishing deformation (i.e., for the CNT at the equilibrium state). Using Eq. (15) and regarding the symmetry $\hat{M}^{FF}_{0_{ijkl}} = \hat{M}^{FF}_{0_{klij}}$ and $\hat{M}^{FG}_{0_{ijklm}} = \hat{M}^{GF}_{0_{klmij}}$, one can achieve the following linear constitutive relation

$$\hat{\mathbf{P}} = \hat{\mathbf{M}}_0^{FF} : \mathbf{F} + \hat{\mathbf{M}}_0^{FG} \vdots \mathbf{G} \quad \text{(Eq. 16-a)}$$

$$\hat{\mathbf{Q}} = \hat{\mathbf{M}}_0^{GF} : \mathbf{F} + \hat{\mathbf{M}}_0^{GG} \vdots \mathbf{G} \quad \text{(Eq. 16-b)}$$

which, as seen, is the linear counterpart of Eqs. (14a-b).

For the special case of a graphene sheet under infinitesimal deformation, the corresponding constitutive relation can be obtained by computing the linear elasticity tensors for $\mathbf{F}=\mathbf{I}_2$ and $\mathbf{G}=\mathbf{0}$ where I_2 denotes a 2-by-2 identity matrix.

3. Deformation mapping of single-walled carbon nanotubes

In the current work, a smooth mapping defined on the reference manifold is employed to describe the overall deformation of the carbon nanotube. This technique has been successfully employed by a few researchers to the study of the mechanical properties of carbon nanotubes [53, 56-58]. Let $\{\mathbf{X}_1, \mathbf{X}_2\}$, $\{\mathbf{I}_1, \mathbf{I}_2\}$ be the Euclidian coordinates and the corresponding orthogonal basis at the reference body (i.e., the unrolled graphene sheet), respectively and $\{\mathbf{x}_1, \mathbf{x}_2, \mathbf{x}_3\}$, $\{\mathbf{i}_1, \mathbf{i}_2, \mathbf{i}_3\}$ separately denote the Euclidian coordinates and the associated orthogonal basis at the current body (i.e., the deformed nanotube). Fig. 2 represents the deformation map ϕ transforming the initial configuration at the space R^2 into the current configuration at the space R^3 as $\mathbf{x}=\boldsymbol{\phi}(\mathbf{x})$.

Consider a (n,m) carbon nanotube of unit ideal length (L_0=1 nm), the ideal radius $R_0 = a_0/2\pi\sqrt{3(n^2+nm+m^2)}$ and chirality $\phi_0 = \arccos\left(\frac{2n+m}{2\sqrt{n^2+m^2+nm}}\right)$. For this CNT, the undeformed body can be defined as $\forall_0 = (0,1)\times(0,2\pi R_0)$. It is assumed that the deformations in the axial and circumferential directions are homogenous. The general deformation mapping from the undeformed body to a cylinder with uniform longitudinal stretch or compression λ_1 and circumferential stretch or compression λ_2 is given by [75]

$$\boldsymbol{\phi}(X) = \lambda_1 X_1\, \mathbf{i}_1 + \lambda_2 R_0 \sin\left(\frac{X_2}{R_0} + \theta\lambda_1 X_1\right) \mathbf{i}_2 + \lambda_2 R_0 \left(1 - \cos\left(\frac{X_2}{R_0} + \theta\lambda_1 X_1\right)\right) \mathbf{i}_3 \quad \text{(Eq. 17)}$$

in which θ is the twisting angle per unit length which physically represents the shear strain. So, for the above described deformation, the deformation gradients are obtained as a function of λ_1, λ_2 and θ. This makes the effective strain energy density

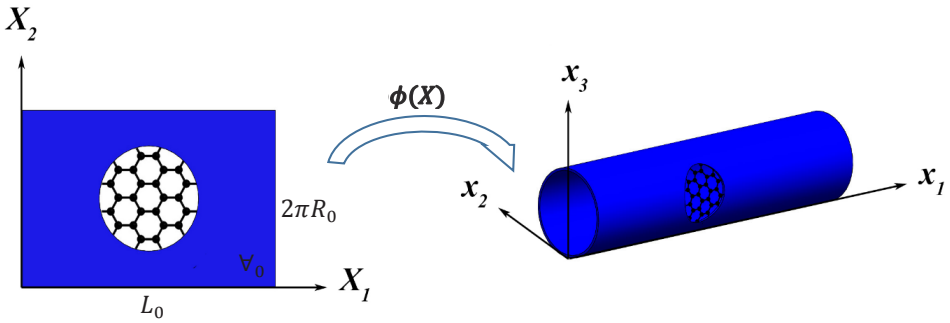

Fig. 2- General transformation mapping from the reference configuration to the current one.

$\widehat{W}(\mathbf{F},\mathbf{G})$ given by Eq. (10) become

$$\widehat{W}(\lambda_1,\lambda_2,\theta) = W\left(\lambda_1,\lambda_2,\theta,\widehat{\boldsymbol{\eta}}(\lambda_1,\lambda_2,\theta)\right) \quad \text{(Eq. 18)}$$

From the previous equation, the deformation is seen to be parameterized by the set (λ_1, λ_2 ,θ).

4. Evaluating elastic properties of single-walled carbon nanotubes

4.1. Nanotube at the equilibrium state

Before any deformation is applied, it is essential to determine the stress free equilibrium state of the carbon nanotube. The atomistic simulations show that the cylinder simply formed by rolling up a planar graphene sheet without stretch or compression (λ_1=λ_2=1) is not in equilibrium. In other words, relaxations in the longitudinal and circumferential directions take place that cause the energy of the nanotube with unit length and ideal radius not to be the minimum energy that a carbon nanotube can reach [53]. Moreover, theoretical results show that a nonzero twisting angle due to rotation deformation (i.e., a rotational relaxation) may occur for CNTs [75]. So, the equilibrium configuration and energetics of a fully relaxed nanotube can be obtained by minimizing the effective strain energy density with respect to the parameters λ_1, λ_2 and θ as

$$\frac{\partial \widehat{W}}{\partial \lambda_1} = \frac{\partial \widehat{W}}{\partial \lambda_2} = \frac{\partial \widehat{W}}{\partial \theta} = 0 \quad \text{(Eq. 19)}$$

By solving Eq. (19) through a numerical approach, the equilibrium values λ_{1eq}, λ_{2eq} and θ_{eq} are determined. Note that the inner relaxation is automatically included in the potential $\widehat{W}$. It means that the minimization for W is performed with respect to five parameters λ_1, λ_2, θ, η_1 and η_2. For a CNT at the equilibrium state, the deformation gradients are then calculated using Eq. (17) for λ_1=λ_{1eq}, λ_2=λ_{2eq} and θ=θ_{eq}. So, the equilibrium radius and length of the nanotube are equal to R=$\lambda_{2eq}R_0$ and L=$\lambda_{1eq}L_0$. Also, at this configuration, the computed elastic properties are applicable in the linear regime or for infinitesimal deformations.

To characterize the axial stiffness of the CNT from the elastic moduli, it must be remarked that which one of the elasticity tensors is the most appropriate to choose. Among the elastic moduli, the appropriate choice is the first elasticity tensor $\widehat{\mathbf{M}}^{FF}$ since its spatial form appears in the linear theory relating the Cauchy stress to the small strain [76]. Accordingly, at the limit of strains approaching zero, the tensile stiffness (or surface Young's modulus) in the axial direction together with the corresponding Poisson's ratio can be obtained by [51, 56, 57, 69]

$$S_a = \widehat{M}^{FF}_{0_{1111}} - \frac{\left(\widehat{M}^{FF}_{0_{1122}}\right)^2}{\widehat{M}^{FF}_{0_{2222}}} \quad \text{(Eq. 20-a)}$$

$$\nu_a = \frac{\widehat{M}^{FF}_{0_{1122}}}{\widehat{M}^{FF}_{0_{2222}}} \quad \text{(Eq. 20-b)}$$

The elasticity tensor $\widehat{\mathbf{M}}^{FF}$ has units of force divided by length. So, phrasing as stiffness is correct and consistent with two-dimensional nature of the CNT. Moreover, the linear tensile stiffness in the circumferential direction can be evaluated as follows

$$S_c = \widehat{M}^{FF}_{0_{2222}} - \frac{\left(\widehat{M}^{FF}_{0_{1122}}\right)^2}{\widehat{M}^{FF}_{0_{1111}}} \quad \text{(Eq. 21)}$$

Penj et al. [77] modeled the SWCNT as an orthotropic thin shell and presented similar expressions in terms of the coefficients of the second elasticity tensor for approximation of the elastic properties of CNTs.

The linear elastic properties of the planar graphene can also be evaluated using the above relationships by considering the elasticity tensor $\widehat{\mathbf{M}}^{FF}_0$ at the reference configuration for which the deformation gradients become $\mathbf{F}=\mathbf{I}_2$ and $\mathbf{G}=\mathbf{0}$. Also, it is clear that for graphene at the equilibrium state, the inner displacement vector $\widehat{\boldsymbol{\eta}}$ vanishes. One noticeable point is that since the elastic modulus for graphene is isotropic, Eqs. (20a) and (21) give the same tensile stiffness.

4.2. Nanotube under axial deformation

A nanotube axially deformed and otherwise unconstrained is considered. The goal is to evaluate the mechanical properties in the axial direction at finite strains. It is assumed that the atoms of the nanotube do not leave the cylindrical surface and as the nanotube is axially deformed, the cylindrical symmetry is not lost.

When the CNT is axially deformed, the Poisson effect leads to the change in the equilibrium radius of the nanotube. In other words, the constant λ_2 in Eq. (17) can be viewed as a radial relaxation parameter. Further, a rotational relaxation θ takes place resulting from the interaction between the axial deformation and the possible twisting deformation. For a given axial deformation characterized by λ_1, the relaxed circumferential and twisting deformations are obtained by minimizing the effective strain energy density with respect to λ_2 and θ as

$$\{\tilde{\lambda}_2(\lambda_1), \tilde{\theta}(\lambda_1)\} = arg\left(\min_{\lambda_2,\theta} \widehat{W}(\lambda_1, \lambda_2, \theta)\right) \rightarrow$$

$$\left.\frac{\partial \widehat{W}}{\partial \lambda_2}\right|_{\lambda_2 = \tilde{\lambda}_2, \theta = \tilde{\theta}} = \left.\frac{\partial \widehat{W}}{\partial \theta}\right|_{\lambda_2 = \tilde{\lambda}_2, \theta = \tilde{\theta}} = 0 \quad \text{(Eq. 22)}$$

Thus, the elastic strain energy density of the continuum can be expressed in terms of the single parameter λ_1 as the imposed deformation i.e.,

$$\widetilde{W}(\lambda_1) = \widehat{W}\left(\lambda_1, \tilde{\lambda}_2(\lambda_1), \tilde{\theta}(\lambda_1)\right) \quad \text{(Eq. 23)}$$

This function is a hyperelastic potential for carbon nanotubes under finite stretches. It also accounts for the finite deformation required to roll up a graphene sheet and different relaxation processes namely radial, rotational and inner relaxations taking place during the axial deformation of a nanotube. According to the above, evaluation of an axially stretched or compressed and otherwise unconstrained nanotube requires the solution of the bivariate minimization problem in Eq. (22) which is numerically performed. For fixed λ_1, rather than the effective potential $\widehat{W}$, the strain energy density W can be considered in a four variables minimization problem as follows

$$\frac{\partial W}{\partial \eta_1} = \frac{\partial W}{\partial \eta_2} = \frac{\partial W}{\partial \lambda_2} = \frac{\partial W}{\partial \theta} = 0 \quad \text{(Eq. 24)}$$

It is worth mentioning that since the deformation is uniform, the inner rearrangements are homogenous as well, i.e., the obtained vector $\hat{\boldsymbol{\eta}}$ is constant in $\forall_0$.

As indicated above, the strain energy density of the CNT can be expressed exclusively in terms of the axial deformation λ_1. In other words, the kinematics assumptions and considering any possible relaxation reduce the configuration space of the carbon nanotube to the single scalar parameter λ_1. This means that the CNT can be viewed as a one-dimensional rod with the hyperelastic potential $\widetilde{W}(\lambda_1)$. In this simple case, one can then achieve the axial stiffness of the nanotube from the second-order derivative of the strain energy density $\widetilde{W}(\lambda_1)$ with respect to λ_1 as

$$S_a = \frac{\partial^2 \widetilde{W}}{\partial \lambda_1^2} \quad \text{(Eq. 25)}$$

The corresponding Poisson's ratio is obtained by the ratio of the circumferential strain e_2 to the axial strain e_1 as follows

$$\nu_a = \frac{e_2}{e_1} \quad \text{(Eq. 26)}$$

in which the strains e_1 and e_2 are calculated relative to the initial configuration of the nanotube as

$$e_1 = \frac{(\lambda_1 - \lambda_{1eq})}{\lambda_{1eq}} \quad \text{(Eq. 27-a)}$$

$$e_2 = \frac{(\tilde{\lambda}_2 - \lambda_{2eq})}{\lambda_{2eq}} \quad \text{(Eq. 27-b)}$$

In summary, once the equilibrium state is known, for a given axial deformation λ_1, the internal, radial and twisting relaxations are first computed by solving Eq. (24). The tangent moduli are then calculated from Eqs. (12a-d) for $\lambda_2 = \tilde{\lambda}_2, \theta = \tilde{\theta}$ and the elastic properties are obtained by employing relationships (25) to (27b).

4.3. Nanotube under hydrostatic pressure

Under hydrostatic pressure, deformation of the CNT along the axial direction is uniform. To simulate the CNT subject to hydrostatic pressure, the deformation mapping presented in Eq. (17) is again adopted. Similar analysis to that of the previous section is done, though the loading case is hear induced by altering the parameter λ_2.

Given a circumferential deformation characterized by λ_2, the Poisson effect and twisting deformation are accounted for by minimizing the strain energy density with respect to λ_1 and θ. Thus, considering the relaxed axial and twisting deformations, one has

$$\{\tilde{\lambda}_1(\lambda_2), \tilde{\theta}(\lambda_2)\} = arg\left(\min_{\lambda_1,\theta} \widehat{W}(\lambda_1, \lambda_2, \theta)\right) \rightarrow$$

$$\left.\frac{\partial \widehat{W}}{\partial \lambda_1}\right|_{\lambda_1 = \tilde{\lambda}_1, \theta = \tilde{\theta}} = \left.\frac{\partial \widehat{W}}{\partial \theta}\right|_{\lambda_1 = \tilde{\lambda}_1, \theta = \tilde{\theta}} = 0 \quad \text{(Eq. 28)}$$

Alternatively, the four variables minimization problem for the function W can be considered as follows

$$\frac{\partial W}{\partial \eta_1} = \frac{\partial W}{\partial \eta_2} = \frac{\partial W}{\partial \lambda_1} = \frac{\partial W}{\partial \theta} = 0 \quad \text{(Eq. 29)}$$

Eq. (28) points out that the strain energy density of the CNT can be expressed in terms of the circumferential deformation λ_2, only as

$$\widetilde{W}(\lambda_2) = \widehat{W}\left(\tilde{\lambda}_1(\lambda_2), \lambda_2, \tilde{\theta}(\lambda_2)\right) \quad \text{(Eq. 30)}$$

This function is a one-dimensional hyperelastic potential for the CNT whose second-order derivative with respect to λ_2 gives the circumferential stiffness as

$$S_c = \frac{\partial^2 \widetilde{W}}{\partial \lambda_2^2} \quad \text{(Eq. 31)}$$

Eqs. (25) and (31) can be expanded analogous to Eqs. (12a-d) and (13a-d) to obtain closed-form expressions for the stiffness parameters in terms of the atomistic potential. The contribution of the inner relaxation should be involved when calculating the above constants. Accordingly, the derived expressions depend on the inner displacements, the radial or axial with rotational relaxations determined by solving the minimization problems mentioned above.

Thus, in contrast to the approaches wherein the finite difference approximation of derivatives are made [15, 16], in the present work, all the derivatives of the interatomic potential function are analytically computed and the only numerical step is the calculation of the equilibrium state and the relaxation parameters, leading to reduction of the computational costs and errors.

5. Results and discussion

In this section, elastic properties and energy of the fully relaxed nanotube, the nanotube under compressive and finite tensile and circumferential strains predicted by the current atomistic-continuum model are presented. The effects of chirality and radius on elastic energy, Poisson's ratio, axial and circumferential stiffness of carbon nanotubes at the equilibrium state are discussed. Also, the variations of the mechanical properties and some coefficients of the tangent moduli with deformation are discussed.

5.1. Validation

To validate the present formulations, several comparison examples are given. The strain energy of fully relaxed nanotubes of varying equilibrium radius relative to the planar graphene ($V_{I_{graphene}} = -7.3756\ eV/atom$) are computed and compared with atomistic calculations results reported in Ref. [50] in Fig. 3. The excellent agreement between the atomistic results and the present ones is noticeable specifically for the nanotubes with radius larger than 0.4 nm (i.e., curvatures smaller than 2.5). However, for small nanotubes (high curvatures), a small difference is observed. Moreover, this figure shows that the strain energy of large enough nanotubes is insensitive to the chirality.

Presented in Table 1 are surface Young's modulus and Poisson's ratio of the planar graphene sheet and a few CNTs at the equilibrium state obtained by the atomistic-continuum model with and without inner relaxations. The results are compared to those of other atomistic-continuum approaches existing in the literature. As seen from this table, there is a good agreement among the results.

As mentioned in Section 4.1, the present formulations for characterizing the constitutive properties from the tangent moduli in the linear regime are analogous to those employed in Refs.

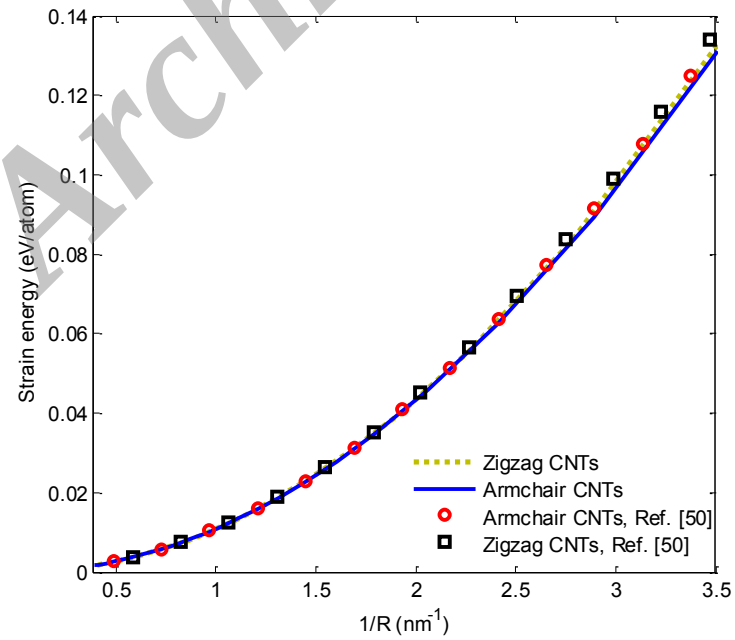

Fig. 3- Comparison of strain energy relative to planar graphene for relaxed armachir and zigzag carbon nanotubes of varying radius.

Table 1- Comparison of elastic properties of planar graphene and carbon nanotubes

Nanostructure	Inner relaxation	Surface Young's modulus in the axial direction ($\frac{nN}{nm}$)				Poisson's ratio		
		Present	Refs. [50, 53]	Ref. [69]	Ref. [4]	Present	Refs. [50, 53]	Ref. [69]
Planar graphene	With	235.88	235.8	236.39	-	0.4135	0.4123	0.4133
	Without	338.54	337.8	339	-	0.1584	0.1580	0.1583
(10,10) CNT	With	233.56	233	-	-	0.4159	0.414	-
	Without	336.43	336	-	-	0.1603	-	-
(5,5) CNT	With	228.08	228	-	224.40	0.4261	0.418	-
(10,0) CNT	With	228.51	225	-	229.26	0.4223	0.419	-
(9,6) CNT	With	232.50	-	-	232.31	0.4188	-	-

[56, 69, 77]. So, one can make a comparison between the coefficients of the linear tangent modulus tensor $\widehat{\mathbf{M}}_0^{FF}$ of the planar graphene and those of the extensional stiffness tensor obtained by the second-order derivatives of the strain energy density with respect to Lagrangian strain (i.e., the second elasticity tensor) in Ref. [69]. Table 2 depicts the results corresponding to the coefficients of these two forth-order elasticity tensors for infinitesimal deformation in the presence and absence of the inner rearrangements. The in-plane elastic moduli of Ref. [70], in which the inner displacements were calculated by the MD simulations, are also presented. As observed, the agreement among the current results and those of Refs. [69, 70] is excellent. This comparison then demonstrates the reliability of the closed-form expressions derived for the tangent moduli. Furthermore, one can see from Tables 1 and 2 a big difference between the results of the models with and without the inner relaxations.

Fig. 4 shows the strain energy relative to the planar graphene for an axially deformed and otherwise unconstrained (10,10) nanotube. For this nanotube, the equilibrium values of the axial, circumferential and rotational deformations are obtained as λ_{1eq}=1.0011923, λ_{2eq}=0.9969522 and θ_{eq}=0. The results are provided with and without consideration of the inner relaxations and compared with those of the atomistic model reported in Ref. [53]. It is observed that the present results agree well with the atomistic calculations demonstrating that the current atomistic-based continuum model can reproduce the exact energetics of axially deformed nanotubes. This figure also depicts an overestimate of the energy by the model without the inner relaxation.

From the results presented above it is found that the inner displacements have significant effect on the elastic properties and energy of the CNT and GS so that without consideration of them, the resulting continuum model is stiffer and therefore

Table 2- Comparison of tangent stiffness coefficients of planar graphene

Approach	$\widehat{M}_{0_{2222}}^{FF}$ ($\frac{nN}{nm}$)		$\widehat{M}_{0_{1122}}^{FF}$ ($\frac{nN}{nm}$)		$\widehat{M}_{0_{1212}}^{FF}$ ($\frac{nN}{nm}$)		$(\widehat{M}_{0_{1111}}^{FF} - \frac{(\widehat{M}_{0_{1122}}^{FF})^2}{\widehat{M}_{0_{2222}}^{FF}})(\frac{nN}{nm})$	
	With inner relaxation	Without inner relaxation	With inner relaxation	Without inner relaxation	With inner relaxation	Without inner relaxation	With inner relaxation	Without inner relaxation
Present	284.56	347.25	117.69	54.99	83.34	146.04	235.88	338.54
Ref. [69]	285.10	347.87	117.83	55.06	83.63	146.40	236.39	339
Ref. [70]	284.56	347.25	117.69	54.99	83.43	146.13	-	-

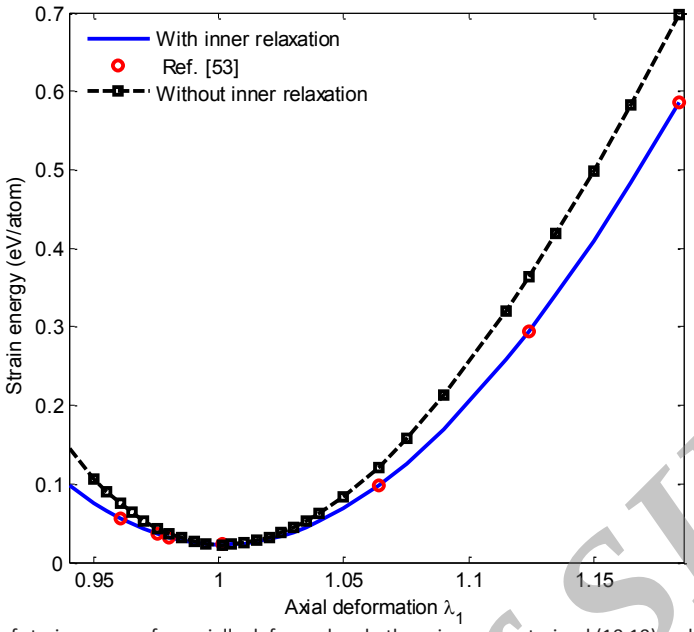

Fig. 4- Comparison of strain energy of an axially deformed and otherwise unconstarined (10,10) carbon nanotube relative to planar graphene

overestimates the stiffness and energy of the nanostructure.

5.2. Elastic properties of fully relaxed CNT

To calculate the equilibrium configuration of a carbon nanotube, the axial and circumferential strains separately denoted by e_{1eq} and e_{2eq} during rolling of the graphene to the CNT versus the ideal radius are plotted in Fig. 5 for armchair, zigzag and chiral nanotubes. In the case of the chiral CNT, the chirality ϕ_0=18° is taken. Also, the strains in percent are computed as follows

$$e_{1eq}=(\lambda_{1eq}-1)\times 100,\ e_{2eq}=(\lambda_{2eq}-1)\times 100$$

It is noted from this figure that the axial strain is small, while the strain in the circumferential

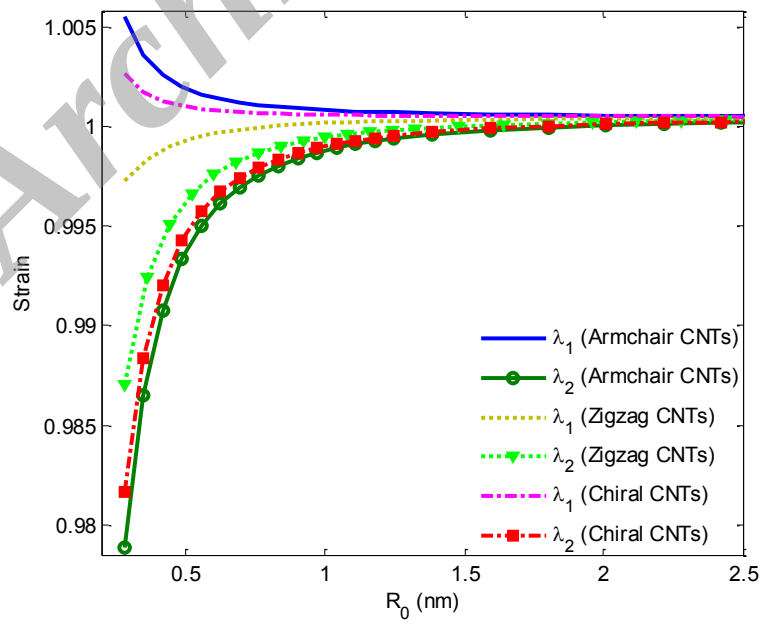

Fig. 5- Equilibrium axial and circumferential strains as a function of the nanotube ideal radius.

direction can reach -2.5% for very small CNT. As the nanotube radius increases, the curves converge and the strains vanish for very large CNT.

Our numerical results also reveal that for the armchair and zigzag nanotubes, the equilibrium twisting angle θ_{eq} vanishes, while it is obtained nonzero for the chiral ones. For example, for (9,6) CNT, the calculated value is equal to θ_{eq}=0.1635682°/nm. The corresponding equilibrium axial and circumferential deformations are also obtained as λ_{1eq}=1.0009996 and λ_{2eq}=0.9941076.

Depicted in Figs. 6 and 7 are separately surface Young's modulus along the axial derection and corresponding Poisson's ratio of several carbon nanotubes with constant ideal radius as a function of chirality. Actually, thanks to the hyperelastic continuum model allowing us to independently choose radius and chirality, the effect of these two parameters on the elastic properties of the CNT is here distinctly described. This is in contrast with the atomistic simulations being limited to the crystallographically admissible nanotubes. From these two figures, a slight but systematic dependence on chirality is observed. It is also seen

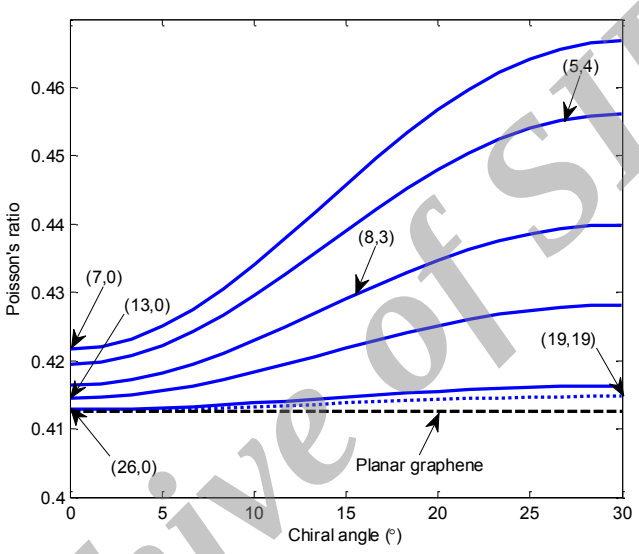

Fig. 7- Poisson's ratio of relaxed carbon nanotubes as a function of chirality

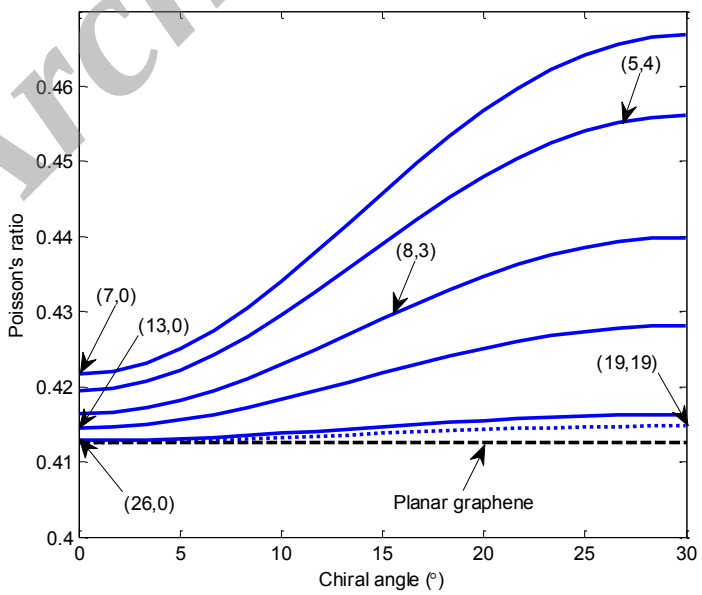

Fig. 6- Tensile stiffnesss of relaxed carbon nanotubes in the axial derection as a function of chirality.

that surface Young's modulus slightly increases with an increase in the radius so that the rate of variations for zigzag nanotube is higher as compared to armchair nanotube and an inverse trend is found for Poisson's ratio. It is because that the imposed curvature weakens the atomic bonds and therefore the smaller nanotubes are softer than the larger ones. Moreover, one can see from Fig. 6 that the largest axial stiffness is obtained for the armchair nanotubes and the smallest stiffness is obtained for the zigzag ones. Similar observation can be made from Fig. 7 about Poisson's ratio of the armchair and zigzag nanotubes. Our observations agree with those reported in Refs. [11, 17, 29, 52, 54].

Depicted in Fig. 8 is variations of circumferential surface Young's modulus with chirality for several fixed ideal radiuses. As observed, similar to the axial modulus, circumferential Young's modulus is systemically dependent on the radius and chirality, though the effect of chirality on this modulus is more significant and the inverse of the effect on axial Young's modulus. Circumferential Young's modulus of armchair CNT is then smaller than that of zigzag one. Moreover, contrary to the axial stiffness, the circumferential stiffness of armchair CNT is more sensitive to the radius than that of zigzag CNT.

One common noticeable point in these three figures is that for smaller nanotubes, the influence of chirality on the elastic properties is found to be stronger. As the radius increases, it becomes less pronounced and a plateau with no dependence on the chirality is reached which corresponds to the planar graphene. This clarifies the issue of the anisotropy of the carbon nanotubes or graphene sheets at finite deformations. In other words, the chirality-dependent results for small nanotubes (i.e., the ones with finite curvature) reveal the anisotropy induced by the finite deformation required to roll up the graphene sheet. As the curvature is reduced (tending to large nanotubes), a small isotropy is acquired and the well-known fact that graphene is isotropic in the infinitesimal regime is manifested.

5.3. Elastic properties of axially deformed and otherwise unconstrained CNT

In this section, the elastic properties of straight nanotube under tension and compression are analyzed. Since the cut-off function in Eq. (6) has a discontinuity at the cut-off distance 0.17nm, its second-order derivatives are then discontinuous and it introduces an abrupt increase in the interatomic potential at this distance. To leave out this unphysical influence of the cut-off function, similar to works [78, 79], the cut-off function is not used here. Since the bifurcation still takes place without the cut-off function, it must be intrinsic to CNTs under tension [79].

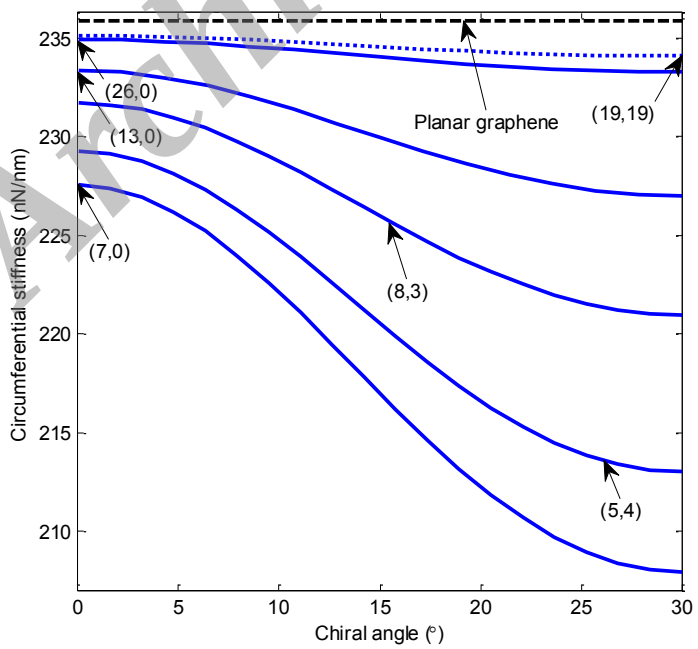

Fig. 8- Tensile stiffness of relaxed carbon nanotubes in the circumferential direction as a function of chirality.

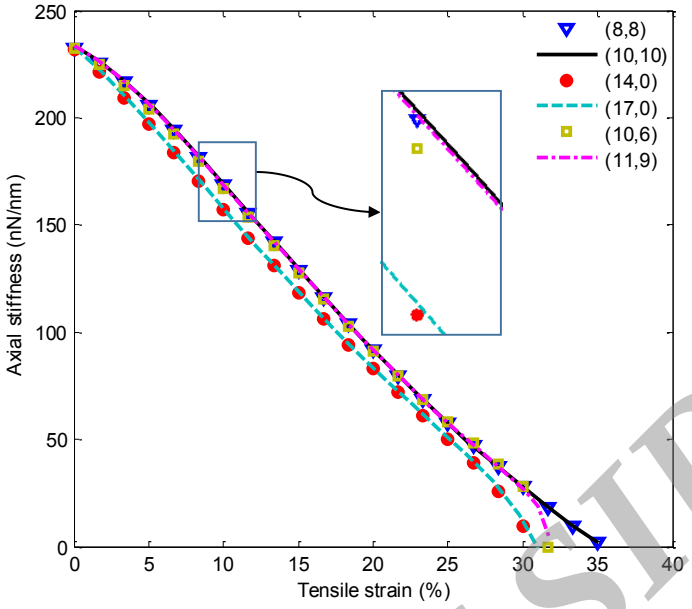

Fig. 9- Axial stiffness of carbon nanotubes under tension as a function of strain.

Fig. 9 indicates variations of axial stiffness with tensile strain for several armchair, zigzag and chiral CNTs. As shown, the axial stiffness monotonically decreases as the stretch increases. Moreover, it can be observed from this figure that the rigidity of the zigzag and armchair nanotubes vanishes at the strains around 31% and 36%, respectively. Following the condition for linear stability of solids reading Y>0 [80] or for the onset of bifurcation when the tangent rigidity reaches zero [81], one can do a simple fracture analysis for the CNTs in tension using Fig. 9. Actually, this figure gives an upper bound on the tensile strain under which the nanotube is stable and has a uniform deformation. It is also observed that the rigidity of the chiral CNTs reaches zero at a strain falling between the critical strains corresponding to the armchair and zigzag CNTs. This is expectable because, as concluded from Fig. 6, tensile strength of the chiral nanotubes is greater than that of zigzag nanotubes and smaller than that of armchair ones. So, according to this figure, the estimated bifurcation strains are between 31-36% which fall in the range reported by MD simulations (30-50% strain) [82] and other atomistic-continuum theories (30-42%) [79] based on the same interatomic potential.

Results presented in Fig. 10 are Poisson's ratio of several armchair, zigzag and chiral CNTs as a function of tensile strain. It is seen that Poisson's ratio of the zigzag nanotubes reaches a minimum value and then increases as the nanotube is further deformed. This behavior is not observed for armchair and chiral CNTs and Poisson's ratio continuously decreases by increasing the tensile strain. At finite strains (e_1>10%), one can see that the influence of chirality on Poisson's ratio of the nanotubes with identical radius such as (4,4), (7,0) and (5,3) CNTs becomes more prominent as the stretch increases.

Axial stiffness of several armchair, zigzag and chiral nanotubes versus compressive strain is plotted in Fig. 11. It is mentioned that in the compression analysis, the results are applicable as long as buckling does not occur. The stiffness is observed to nonlinearly vary with compression which can be attributed to the nonlinearities resulting from the interatomic interactions and considered kinematics. For slightly compressive strains, the rigidity of the armchair and chiral nanotubes reaches a maximum value and then diminishes as the nanotube is further compressed, while such a behavior cannot be observed for the zigzag nanotube. However, for small deformations, it is discerned that each of the three nanotubes represents a hardening behavior. It is found from this figure that the axial stiffness of the zigzag nanotube is more sensitive to the compressive strain than the two other types of the tubes. The greater effect of chirality on nanotubes of the same radius at larger strains is also apparent.

The effect of axial strain on tangent moduli coefficients of three carbon nanotubes with identical

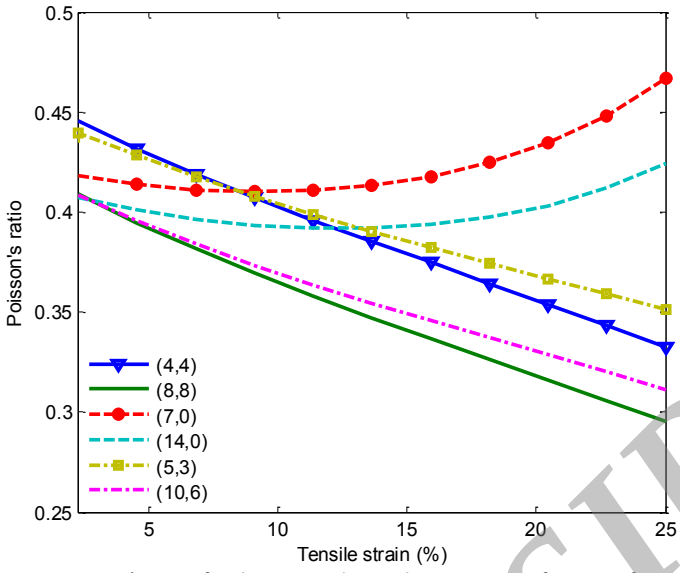

Fig. 10- Poisson's ratio of carbon nanotubes under tension as a function of strain.

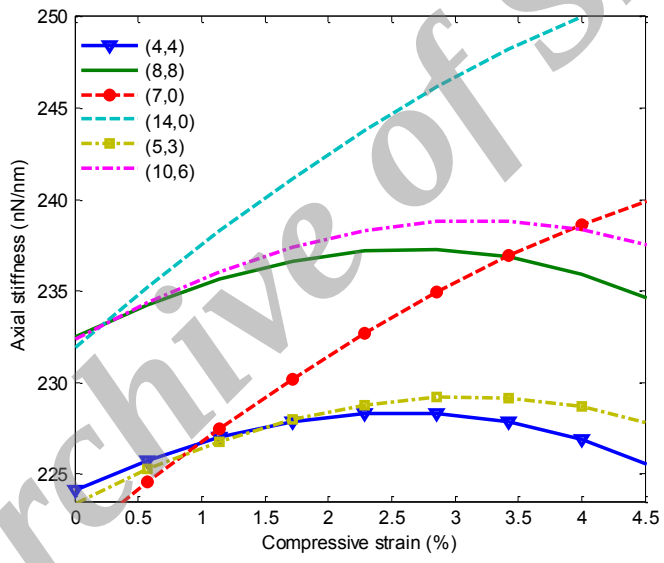

Fig. 11- Axial stiffness of carbon nanotubes under compression as a function of strain.

radius is shown in Fig. 12. One can see from Fig. 12(a) that the coefficients of the first elasticity tensor decrease with an increase in the tensile strain. This behavior implies a material softening which occurs for a nanotube when subjected to the axial tension as reflected in the behavior of the axial stiffness (see Fig. 9). For compressive deformation, one can observe that as the strain increases, the stiffness coefficients $(M^{FF}_{1111}, M^{FF}_{2222}, M^{FF}_{1122})$ slightly increase, too. In contrast, the coefficient M^{FF}_{1212} of the zigzag nanotube slightly decreases by increasing the strain and that of the armchair and chiral nanotubes remains nearly unchanged. Moreover, Fig. 12(a) indicates that at larger axial strains, the effect of chirality on the stiffness coefficients is more prominent. From Figs. 12(b) to (c), it is noted that the coefficients of tangent moduli vary with axial deformation in a nonlinear manner. As a general finding, the CNT possesses a material nonlinearity behavior due to the atomic interactions as reflected in the behavior of the tangent moduli. This nonlinearity is incorporated into the incremental constitutive relation given by Eqs. (14a-b) through calculating the tangent rigidities directly from the interatomic potential. Moreover, as expected, Figs. (12b) and (12c) show that the stiffness coefficients $(M^{FG}_{11311}, M^{GF}_{31111})$ and $(M^{FG}_{22322}, M^{GF}_{32222})$ are mutually equal.

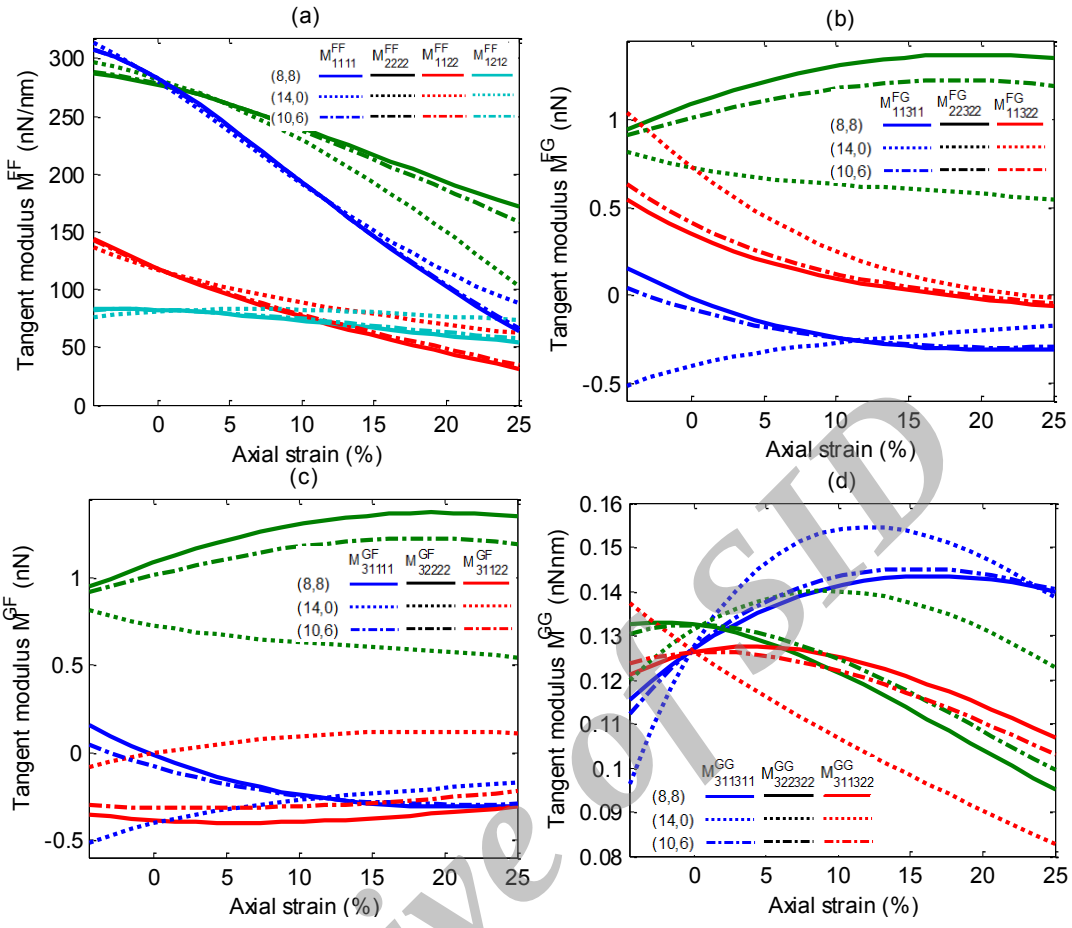

Fig. 12- Tangent moduli coefficients of carbon nanotubes under axial deformation as a fucntion of strain (a) $\mathbf{M}^{FF}$ (b) $\mathbf{M}^{FG}$ (c) $\mathbf{M}^{GF}$ (d) $\mathbf{M}^{GG}$.

5.4. Elastic properties of CNT under hydrostatic pressure

The effect of circumferential strain on the elastic energy, the tensile stiffness and tangent moduli coefficients of the carbon nanotubes under hydrostatic pressure is investigated.

Fig. 13 depicts the strain energy relative to planar graphene for several nanotubes as a function of circumferential deformation. One can see that the strain energy is nearly independent of chirality at small deformations. As the deformation increases, a slight dependence on the chirality is observed so that at large stretches (λ_2>1.3 i.e., by approaching the bifurcation strain) the gap among the curves widens. It is seen that the concavity of the curves corresponding to the zigzag nanotubes is higher than the one corresponding to the armchair nanotubes specially at λ_2>1.3. Based on Eq. (31), it can be qualitatively concluded that the tensile stiffness and then the bifurcation strain for the zigzag CNTs in the circumferential direction is higher than that of the armchair CNTs. To illustrate this, the circumferential stiffness of several nanotubes subject to internal pressure against the circumferential strain is plotted in Fig. 14. It is noted that with an increase in the strain, the stiffness decreases implying a material softening in the circumferential direction for the CNT when subjected to internal pressure. Using this figure, a simple analysis of tensile instability along the circumferential direction similar to the one in the axial tension can be carried out. Accordingly, the strain at which the tensile rigidity reaches zero can be considered as the critical strain for bifurcation. Indeed, at this critical point, the bond length is close to or may go beyond the radius of atomic potential and the CNT cannot undergo deformation anymore and therefore, the stiffness vanishes. The numerical results show that the tensile stiffness vanishes at strains of around 31.5% for armchair CNTs, around

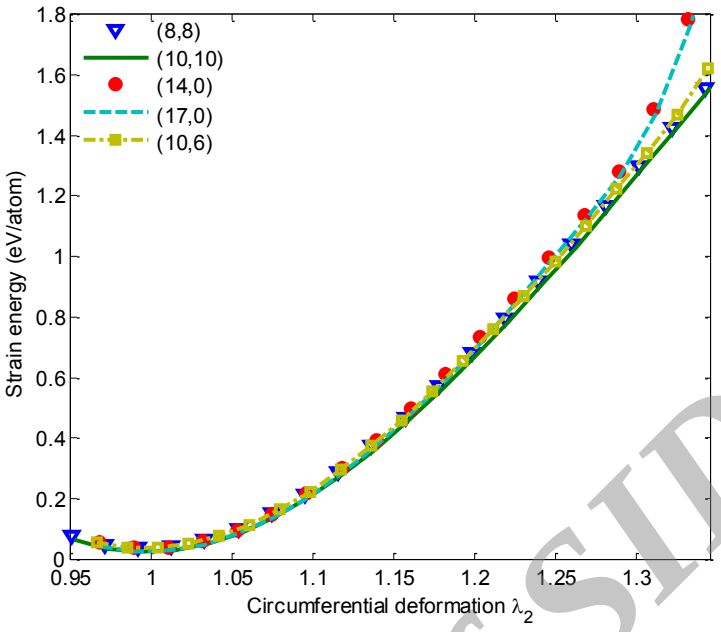

Fig. 13- Strain energy of carbon nanotubes under hydrostatic presure relative to planar graphene.

32.5% for chiral and around 35.5% for zigzag ones. As observed, in contrast with the axial tension instability, the circumferential critical strain for zigzag nanotubes is obtained larger than the one for armchair nanotubes. The reason is related to the tensile strength of the CNT in the circumferential direction that is higher for zigzag nanotube as discerned from Fig. 8. These findings confirm the observation made from the previous figure about the concavity of the curves corresponding to the various chiralities.

Variations of tangent moduli coefficients of three carbon nanotubes with identical radius under internal pressure with circumferential strain are indicated in Fig. 15. It is observed from Fig. 15(a) that the coefficients of the elasticity tensor $\mathbf{M}^{FF}$ diminish by increasing the strain from which the material softening that occurs in the circumferential direction can be inferred. Furthermore, the gap between the curves corresponding to different chiralities is found to increase at finite strains. In other words, the chirality has more important

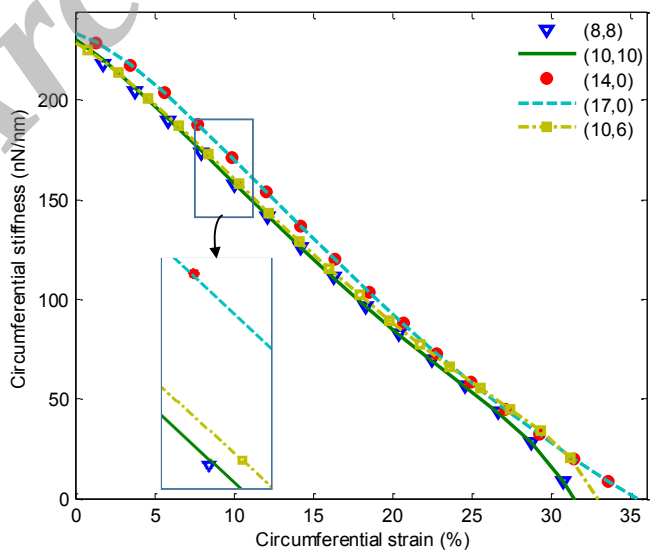

Fig. 14- Cicumferential stiffness of carbon nanotubes under internal presure as a function of strain.

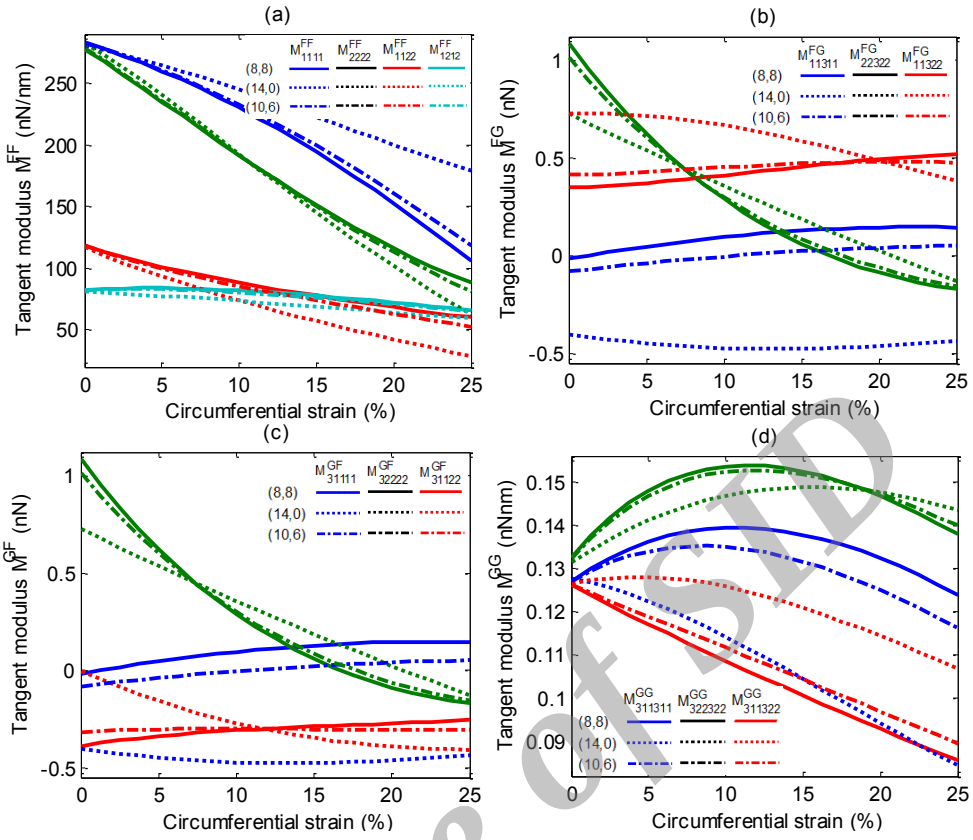

Fig. 15- Tangent moduli coefficients of carbon nanotubes under internal pressure as a fucntion of strain (a) $\mathbf{M}^{FF}$ (b) $\mathbf{M}^{FG}$ (c) $\mathbf{M}^{GF}$ (d) $\mathbf{M}^{GG}$.

influence on the coefficients of the modulus $\mathbf{M}^{FF}$ at large stretches. Figs. 15(b) to 15(c) represent the nonlinear behavior of the coefficients of the tangent moduli versus the circumferential strain implying the material nonlinearity behavior of the carbon nanotubes which are exactly reflected in the constitutive relation. Further, similar to axial tension, the variations of the stiffness coefficients $(M^{FG}_{11311}, M^{GF}_{31111})$ and $(M^{FG}_{22322}, M^{GF}_{32222})$ are mutually the same.

6. Conclusion

A finite deformation membrane model based on the higher-order Cauchy-Born rule along with the deformation mapping technique was employed to study the elastic properties of carbon nanotubes. The material nonlinearity is exactly reflected in the constitutive relation by calculating the elastic moduli of the CNT from the interatomic potential. The model accounts for the important effects of the chirality and different relaxations taking place in a CNT when axially deformed or subjected to hydrostatic pressure. The isolated effects of chirality, radius, axial and circumferential deformations on the elastic properties were described. Comparison with full atomistic and other coupled methods showed that the present model can reproduce the energetics and elastic properties of CNTs with a good accuracy. Main conclusions of the current study are summarized below:

In contrast with the planar graphene, a CNT displays an anisotropic behavior. Degree of anisotropy increases at finite deformations and small radiuses and decreases with an increase in the radius.

The effect of radius on Poisson's ratio and circumferential Young's modulus for armchair CNT is more pronounced than that for zigzag CNT and it is vice versa about axial Young's modulus.

The influence of chirality on the surface Young's modulus in the circumferential direction is more prominent than that in the axial direction.

Due to the nonlinearities coming from the interatomic interactions and kinematics, constitutive properties of the CNT can vary with deformation in a nonlinear manner.

From the analysis of axial and circumferential stiffness against stretch, an upper bound on the tensile strain of the CNTs is obtained.

When subjected to internal pressure, bifurcation takes place in the circumferential direction for armchair CNT sooner than zigzag CNT and it is vice versa when subjected to axial tension.

The armchair and chiral tubes represent a maximum stiffness for slightly compressive deformation. A softening type of tension response at finite strains is observed for all types of the carbon nanotubes.

References:

1. Iijima S. Helical microtubules of graphitic carbon. Nature. 1991;354(6348):56.
2. Bethune DS, Klang CH, De Vries MS, Gorman G, Savoy R, Vazquez J, Beyers R. Cobalt-catalysed growth of carbon nanotubes with single-atomic-layer walls. Nature. 1993;363(6430):605-7.
3. Zakeri M, Shayanmehr M. On the mechanical properties of chiral carbon nanotubes. Journal of Ultrafine Grained and Nanostructured Materials. 2013;46(1):1-9.
4. Chandraseker K, Mukherjee S. Atomistic-continuum and ab initio estimation of the elastic moduli of single-walled carbon nanotubes. Computational Materials Science. 2007;40(1):147-58.
5. Treacy MJ, Ebbesen TW, Gibson JM. Exceptionally high Young's modulus observed for individual carbon nanotubes. Nature. 1996;381(6584):678.
6. Krishnan A, Dujardin E, Ebbesen TW, Yianilos PN, Treacy MM. Young's modulus of single-walled nanotubes. Physical Review B. 1998;58(20):14013.
7. Lourie O, Wagner HD. Evaluation of Young's modulus of carbon nanotubes by micro-Raman spectroscopy. Journal of Materials Research. 1998;13(09):2418-22.
8. Muster J, Burghard M, Roth S, Duesberg GS, Hernandez E, Rubio A. Scanning force microscopy characterization of individual carbon nanotubes on electrode arrays. Journal of Vacuum Science & Technology B: Microelectronics and Nanometer Structures Processing, Measurement, and Phenomena. 1998;16(5):2796-801.
9. Salvetat JP, Briggs GA, Bonard JM, Bacsa RR, Kulik AJ, Stöckli T, Burnham NA, Forró L. Elastic and shear moduli of single-walled carbon nanotube ropes. Physical Review Letters. 1999;82(5):944.
10. Yu MF, Files BS, Arepalli S, Ruoff RS. Tensile loading of ropes of single wall carbon nanotubes and their mechanical properties. Physical Review Letters. 2000;84(24):5552.
11. Hernandez E, Goze C, Bernier P, Rubio A. Elastic properties of single-wall nanotubes. Applied Physics A: Materials Science & Processing. 1999;68(3):287-92.
12. Goze C, Vaccarini L, Henrard L, Bernier P, Hemandez E, Rubio A. Elastic and mechanical properties of carbon nanotubes. Synthetic Metals. 1999;103(1-3):2500-1.
13. Vaccarini L, Goze C, Henrard L, Hernandez E, Bernier P, Rubio A. Mechanical and electronic properties of carbon and boron–nitride nanotubes. Carbon. 2000;38(11):1681-90.
14. Sánchez-Portal D, Artacho E, Soler JM, Rubio A, Ordejón P. Ab initio structural, elastic, and vibrational properties of carbon nanotubes. Physical Review B. 1999;59(19):12678-88.
15. Kudin KN, Scuseria GE, Yakobson BI. C 2 F, BN, and C nanoshell elasticity from ab initio computations. Physical Review B. 2001;64(23):235406.
16. Van Lier G, Van Alsenoy C, Van Doren V, Geerlings P. Ab initio study of the elastic properties of single-walled carbon nanotubes and graphene. Chemical Physics Letters. 2000;326(1):181-5.
17. Robertson DH, Brenner DW, Mintmire JW. Energetics of nanoscale graphitic tubules. Physical Review B. 1992;45(21):12592.
18. Overney G, Zhong W, Tomanek D. Structural rigidity and low frequency vibrational modes of long carbon tubules. Zeitschrift für Physik D Atoms, Molecules and Clusters. 1993;27(1):93-6.
19. Yakobson BI, Brabec CJ, Bernholc J. Nanomechanics of carbon tubes: instabilities beyond linear response. Physical Review Letters. 1996;76(14):2511.
20. Cornwell CF, Wille LT. Elastic properties of single-walled carbon nanotubes in compression. Solid State Communications. 1997;101(8):555-8.
21. Halicioglu T. Stress calculations for carbon nanotubes. Thin Solid Films. 1998;312(1):11-4.
22. Lu JP. Elastic properties of carbon nanotubes and nanoropes. Physical Review Letters. 1997;79(7):1297.
23. Prylutskyy YI, Durov SS, Ogloblya OV, Buzaneva EV, Scharff P. Molecular dynamics simulation of mechanical, vibrational and electronic properties of carbon nanotubes. Computational Materials Science. 2000;17(2):352-5.
24. Jin Y, Yuan FG. Simulation of elastic properties of single-walled carbon nanotubes. Composites Science and Technology. 2003;63(11):1507-15.
25. Kwon YK, Berber S, Tománek D. Thermal contraction of carbon fullerenes and nanotubes. Physical Review Letters. 2004;92(1):015901.
26. Agrawal PM, Sudalayandi BS, Raff LM, Komanduri R. A comparison of different methods of Young's modulus determination for single-wall carbon nanotubes (SWCNT) using molecular dynamics (MD) simulations. Computational Materials Science. 2006;38(2):271-81.
27. DiBiasio CM, Cullinan MA, Culpepper ML. Difference between bending and stretching moduli of single-walled carbon nanotubes that are modeled as an elastic tube. Applied Physics Letters. 2007;90(20):203116.
28. Hu N, Jia B, Arai M, Yan C, Li J, Liu Y, Atobe S, Fukunaga H. Prediction of thermal expansion properties of carbon nanotubes using molecular dynamics simulations. Computational Materials Science. 2012;54:249-54.
29. Bian L, Zhao H. Elastic properties of a single-walled carbon nanotube under a thermal environment. Composite Structures. 2015;121:337-43.
30. Li T, Tang Z, Huang Z, Yu J. A comparison between the mechanical and thermal properties of single-walled carbon nanotubes and boron nitride nanotubes. Physica E: Low-dimensional Systems and Nanostructures. 2017;85:137-42.
31. Eringen AC. On differential equations of nonlocal elasticity and solutions of screw dislocation and surface waves. Journal of Applied Physics. 1983;54(9):4703-10.

32. Eringen AC. Nonlocal continuum field theories. Springer Science & Business Media; 2002.

33. Mindlin RD, Tiersten HF. Effects of couple-stresses in linear elasticity. Archive for Rational Mechanics and analysis. 1962;11(1):415-48.

34. Toupin RA. Theories of elasticity with couple-stress. Archive for Rational Mechanics and Analysis. 1964;17(2):85-112.

35. Aifantis EC. Gradient deformation models at nano, micro, and macro scales. Journal of Engineering Materials and Technology. 1999;121(2):189-202.

36. Lam DC, Yang F, Chong AC, Wang J, Tong P. Experiments and theory in strain gradient elasticity. Journal of the Mechanics and Physics of Solids. 2003;51(8):1477-508.

37. Wang CM, Zhang YY, He XQ. Vibration of nonlocal Timoshenko beams. Nanotechnology. 2007;18(10):105401.

38. Reddy JN, Pang SD. Nonlocal continuum theories of beams for the analysis of carbon nanotubes. Journal of Applied Physics. 2008;103(2):023511.

39. Hu YG, Liew KM, Wang Q, He XQ, Yakobson BI. Nonlocal shell model for elastic wave propagation in single-and double-walled carbon nanotubes. Journal of the Mechanics and Physics of Solids. 2008;56(12):3475-85.

40. Murmu T, Pradhan SC. Thermo-mechanical vibration of a single-walled carbon nanotube embedded in an elastic medium based on nonlocal elasticity theory. Computational Materials Science. 2009;46(4):854-9.

41. Civalek Ö, Akgöz B. Static analysis of single walled carbon nanotubes (SWCNT) based on Eringen's nonlocal elasticity theory. International Journal of Engineering and Applied Sciences. 2009;1(2):47-56.

42. Yang J, Ke LL, Kitipornchai S. Nonlinear free vibration of single-walled carbon nanotubes using nonlocal Timoshenko beam theory. Physica E: Low-dimensional Systems and Nanostructures. 2010;42(5):1727-35.

43. Lim CW, Yang Y. New predictions of size-dependent nanoscale based on nonlocal elasticity for wave propagation in carbon nanotubes. Journal of Computational and Theoretical Nanoscience. 2010;7(6):988-95.

44. Akgöz B, Civalek Ö. Buckling analysis of cantilever carbon nanotubes using the strain gradient elasticity and modified couple stress theories. Journal of Computational and Theoretical Nanoscience. 2011;8(9):1821-7.

45. Yang Y, Zhang L, Lim CW. Wave propagation in fluid-filled single-walled carbon nanotube on analytically nonlocal Euler–Bernoulli beam model. Journal of Sound and Vibration. 2012;331(7):1567-79.

46. Demir Ç, Civalek Ö. Nonlocal finite element formulation for vibration. International Journal of Engineering and Applied Sciences. 2016;8:109-17.

47. Civalek Ö, Demir C. A simple mathematical model of microtubules surrounded by an elastic matrix by nonlocal finite element method. Applied Mathematics and Computation. 2016;289:335-52.

48. Akgöz B, Civalek Ö. Bending analysis of embedded carbon nanotubes resting on an elastic foundation using strain gradient theory. Acta Astronautica. 2016;119:1-2.

49. Shahabodini A, Ansari R, Darvizeh M. Multiscale modeling of embedded graphene sheets based on the higher-order Cauchy-Born rule: Nonlinear static analysis. Composite Structures. 2017;165:25-43.

50. Arroyo M, Belytschko T. Finite crystal elasticity of carbon nanotubes based on the exponential Cauchy-Born rule. Physical Review B. 2004;69(11):115415.

51. Zhang P, Huang Y, Geubelle PH, Klein PA, Hwang KC. The elastic modulus of single-wall carbon nanotubes: a continuum analysis incorporating interatomic potentials. International Journal of Solids and Structures. 2002;39(13):3893-906.

52. Arroyo M, Belytschko T. Large deformation atomistic-based continuum analysis of carbon nanotubes. In 43rd AIAA/ASME/ASCE/AHS/ASC Structures, Structural Dynamics, and Materials Conference, 2002.

53. Arroyo M. Finite crystal elasticity for curved single layer lattices: applications to carbon nanotubes. PhD dissertation, Northwestern University, USA, 2003.

54. Jiang H, Zhang P, Liu B, Huang Y, Geubelle PH, Gao H, Hwang KC. The effect of nanotube radius on the constitutive model for carbon nanotubes. Computational Materials Science. 2003;28(3):429-42.

55. Jiang H, Huang Y, Hwang KC. A finite-temperature continuum theory based on interatomic potentials. Journal of Engineering Materials and Technology. 2005;127(4):408-16.

56. Guo X, Wang JB, Zhang HW. Mechanical properties of single-walled carbon nanotubes based on higher order Cauchy–Born rule. International Journal of Solids and Structures. 2006;43(5):1276-90.

57. Wang JB, Guo X, Zhang HW, Wang L, Liao J. Energy and mechanical properties of single-walled carbon nanotubes predicted using the higher order Cauchy-Born rule. Physical Review B. 2006;73(11):115428.

58. Guo X, Zhang T. A study on the bending stiffness of single-walled carbon nanotubes and related issues. Journal of the Mechanics and Physics of Solids. 2010;58(3):428-43.

59. Guo X, Liao J, Wang X. Investigation of the thermo-mechanical properties of single-walled carbon nanotubes based on the temperature-related higher order Cauchy–Born rule. Computational Materials Science. 2012;51(1):445-54.

60. Ansari R, Shahabodini A, Alipour A, Rouhi H. Stability of a single-layer graphene sheet with various edge conditions: a non-local plate model including interatomic potentials. Proceedings of the Institution of Mechanical Engineers, Part N: Journal of Nanoengineering and Nanosystems. 2012;226(2):51-60.

61. Ansari R, Shahabodini A, Rouhi H. Prediction of the biaxial buckling and vibration behavior of graphene via a nonlocal atomistic-based plate theory. Composite Structures. 2013;95:88-94.

62. Ansari R, Shahabodini A, Rouhi H. A nonlocal plate model incorporating interatomic potentials for vibrations of graphene with arbitrary edge conditions. Current Applied Physics. 2015;15(9):1062-9.

63. Ansari R, Shahabodini A, Rouhi H. A thickness-independent nonlocal shell model for describing the stability behavior of carbon nanotubes under compression. Composite Structures. 2013;100:323-31.

64. Ansari R, Shahabodini A, Rouhi H, Alipour A. Thermal buckling analysis of multi-walled carbon nanotubes through a nonlocal shell theory incorporating interatomic potentials. Journal of Thermal Stresses. 2013;36(1):56-70.

65. Giannopoulos GI, Kakavas PA, Anifantis NK. Evaluation of the effective mechanical properties of single walled carbon nanotubes using a spring based finite element approach.

Computational Materials Science. 2008;41(4):561-9.

66. Ghavamian A, Rahmandoust M, Öchsner A. On the determination of the shear modulus of carbon nanotubes. Composites Part B: Engineering. 2013;44(1):52-9.

67. Mohammadpour E, Awang M. Predicting the nonlinear tensile behavior of carbon nanotubes using finite element simulation. Applied Physics A: Materials Science & Processing. 2011;104(2):609-14.

68. Sakharova NA, Pereira AF, Antunes JM, Fernandes JV. Numerical simulation study of the elastic properties of single-walled carbon nanotubes containing vacancy defects. Composites Part B: Engineering. 2016;89:155-68.

69. Singh S, Patel BP. Nonlinear elastic properties of graphene sheet under finite deformation. Composite Structures. 2015;119:412-21.

70. Zhou J, Huang R. Internal lattice relaxation of single-layer graphene under in-plane deformation. Journal of the Mechanics and Physics of Solids. 2008;56(4):1609-23.

71. Lu Q, Huang R. Nonlinear mechanics of single-atomic-layer graphene sheets. International Journal of Applied Mechanics. 2009;1(03):443-67.

72. Lu Q, Arroyo M, Huang R. Elastic bending modulus of monolayer graphene. Journal of Physics D: Applied Physics. 2009;42(10):102002.

73. Tersoff J. New empirical approach for the structure and energy of covalent systems. Physical Review B. 1988;37(12):6991.

74. Brenner DW. Empirical potential for hydrocarbons for use in simulating the chemical vapor deposition of diamond films. Physical Review B. 1990;42(15):9458.

75. Wang X, Guo X. Numerical simulation for finite deformation of single-walled carbon nanotubes at finite temperature using temperature-related higher order Cauchy-Born rule based quasi-continuum model. Computational Materials Science. 2012;55:273-83.

76. Belytschko T, Liu WK, Moran B, Elkhodary K. Nonlinear finite elements for continua and structures. John wiley & sons; 2013.

77. Peng J, Wu J, Hwang KC, Song J, Huang Y. Can a single-wall carbon nanotube be modeled as a thin shell?. Journal of the Mechanics and Physics of Solids. 2008;56(6):2213-24.

78. Belytschko T, Xiao SP, Schatz GC, Ruoff RS. Atomistic simulations of nanotube fracture. Physical Review B. 2002;65(23):235430.

79. Zhang P, Jiang H, Huang Y, Geubelle PH, Hwang KC. An atomistic-based continuum theory for carbon nanotubes: analysis of fracture nucleation. Journal of the Mechanics and Physics of Solids. 2004;52(5):977-98.

80. Hill R. On the elasticity and stability of perfect crystals at finite strain. In Mathematical Proceedings of the Cambridge Philosophical Society. 1975;77(1):225-40.

81. Song J, Wu J, Huang Y, Hwang KC. Continuum modeling of boron nitride nanotubes. Nanotechnology. 2008;19(44):445705.

82. Yakobson BI, Campbell MP, Brabec CJ, Bernholc J. High strain rate fracture and C-chain unraveling in carbon nanotubes. Computational Materials Science. 1997;8(4):341-8.